THE B REGIONAL DUST STORM IN THE NEW NASA AMES MARS GCM.

C.M.L. Batterson, *Bay Area Environmental Research Institute, Moffett Field, CA, USA (courtney.m.batterson@nasa.gov)*, **M.A.Kahre,** *NASA Ames Research Center, Moffett Field, CA, USA*, **A.F.C. Bridger,** *Department of Meteorology, San Jose State University, San Jose, CA, USA*, **R.J.Wilson,** *NASA Ames Research Center, Moffett Field, CA, USA*, **R.A.Urata,** *Bay Area Environmental Research Institute, Moffett Field, CA, USA*.

Introduction

The Thermal Emission Spectrometer (TES) and the Mars Climate Sounder (MCS) instruments have been observing global dust and temperature on Mars twice daily for a combined ∼12 Mars Years (MYs). Analysis of these data by [5] reveal three highly repeatable, regional scale dust events occurring annually during years lacking a global dust storm (GDS). Named the "A," "B," and "C" storms in seasonal order, these recurring dust storms develop in the southern hemisphere of Mars during the perihelion season (L_s =180°–360°) when Mars is closest to the sun and the southern hemisphere experiences summer [5]. The "A" and "C" storms occur in the southern midlatitudes where they amplify the Hadley circulation causing dynamical warming in the northern hemisphere. In contrast, the "B" storm (hereafter, B storm) and its effects are entirely confined to the south pole [5]. All three storms are large enough to inject dust above the boundary layer [8]. As a result, the annually-recurring regional storms produce significant temperature perturbations in the middle atmosphere, raising zonal mean 50 Pa (25 km) temperatures above 200 K (Figure 1) [5].

In this work, we seek to identify the mechanisms responsible for lofting dust into the middle atmosphere during the B storm by simulating the storm with the new NASA Ames Mars Global Climate Model (MGCM). We find that the simulated B storm is driven by a series of dust plumes that form in the high southern latitudes during southern summer solstice. We also find that radiative-dynamic feedbacks between airborne dust and incoming shortwave radiation are crucial for the pluming mechanism.

Methods

We simulate the B storm using the new NASA Ames MGCM with the finite-volume dynamical core and cubed-sphere grid developed by NOAA/GFDL. Model topography is derived from high-resolution (1/16°) Mars Orbiter Laser Altimeter (MOLA) retrievals while surface thermal inertia and albedo are derived from TES observations [7, 10]. The seasonal growth and recession of the north and south polar ice caps maintain a surface energy balance that is dependent, in part, on the albedo prescribed to each. We use the nominal albedos of 0.7 and 0.51 for the north and south polar caps, respectively, which we find to produce a good fit to the Viking Lander-observed surface pressure cycle.

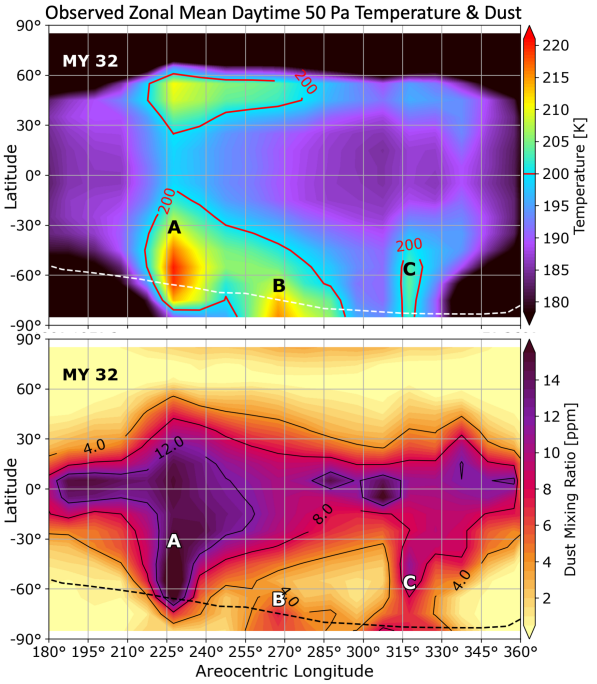

Figure 1: Observed zonal mean daytime (3 PM) 50 Pa temperatures (top) and dust mixing ratios (bottom) for L_s = 180°–360° in MY32. The red contour is the 200 K isotherm and the dashed line marks the northernmost edge of the receding CO_2 ice cap.

Water ice cloud microphysics are excluded from our simulations, but the radiative properties of dust and gaseous CO_2 are included in a 2-stream RT scheme [3, 9]. Gaseous opacities for CO_2 are calculated from correlated-k tables and Rayleigh scattering for CO_2 is computed directly. The optical properties of dust depend on the particle size distribution of dust in the atmosphere. In the MGCM, dust mass and number mixing ratios are carried as tracers and used to compute the temporally and spatially-evolving effective particle size distribution. The optical properties of the dust are calculated from Mie theory and then weighted according to the size distribution of the aerosol [3].

Dust aerosols are a major source of radiative forcing on Mars and their effects are largely dependent on the size distribution of dust in the atmosphere [11]. In the MGCM, the size distribution of the lifted dust particles is determined by a user-assigned effective radius (r_{eff}), and airborne dust is then allowed to evolve, radi-

ate, be transported by resolved winds, and sediment out due to gravity [3]. The MGCM dust lifting scheme is constrained by a set of daily global dust column opacity maps from [6], which are used to indicate when and where dust should be injected into the lowest model layer [3, 11].

The MGCM was run at ∼1°x1° (∼60x60 km) horizontal resolution with a terrain-following, 30-layer hybrid σ-pressure vertical coordinate featuring a ∼6 m vertical resolution near the surface and ∼10 km resolution near the top (∼90 km). The MY31 daily global dust opacity maps were used to inform the dust lifting scheme, and the lifted particle effective radius was set to r_{eff} =3 μm , which was the same value used to reproduce the MY34 GDS in the MGCM and which we find reasonably reproduces the observed B storm [6, 1]. The MGCM was run for two years, and output from the second half (L_s =180°–360°) of the second year was analyzed in this study.

Results

The behavior of the simulated B storm closely follows that of the observed B storm. The simulated B storm occurs poleward of 60° S during southern summer solstice as observed, and its growth phase is marked by a rapid increase in middle atmospheric temperatures and dust concentrations. Figure 2 shows that 50 Pa B storm temperatures maximize at ∼15 K above normal just before solstice and exceed 200 K for ∼10° of L_s around solstice. Corresponding dust mixing ratios exceed 4 ppm during the same period, maximizing near ∼6 ppm. After solstice, the simulated B storm slowly decays as dust falls out of suspension allowing temperatures to return to normal ∼15° of L_s after the storm's peak. Overall, the simulated B storm is shorter-lived (and somewhat weaker) than observed, but it nonetheless meets the criteria for a B storm event: 50 Pa temperatures exceed 200 K, 50 Pa dust exceed 4 ppm, there is no northern hemisphere response, and the storm maximizes around southern summer solstice (L_s =270°) [5].

The simulated global mean thermal and dynamical structure of the southern summer atmosphere are shown in Figure 3. Simulated temperatures reflect a large near-surface thermal gradient with a maximum of just over 240 K at the south pole and a minimum of 140–150 K at the north pole. There is a northward-tilting column of warm air over the winter pole and a steep thermal gradient through the column over the south pole. The simulated atmosphere is somewhat cooler than observed in parts of the upper atmosphere, however, temperatures in the lower and middle atmosphere are comparable to the observed environment. The zonal mean overturning circulation is dominated by a cross-equatorial Hadley cell with a rising branch located around 40° S and a sinking branch over ∼60° N. The southern summer Hadley cell lofts dust tens of kilometers and disperses it globally [4]. However, the B storm is located tens of degrees

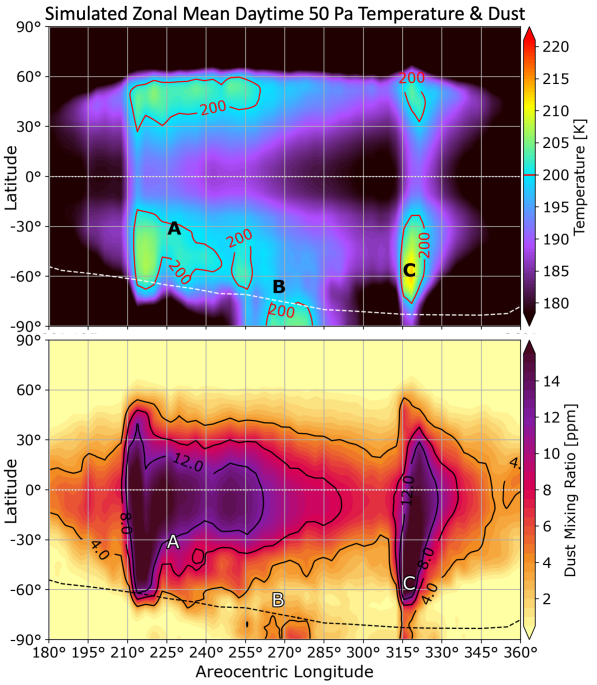

Figure 2: As in Figure 1 but for simulated temperatures and dust mixing ratios.

in latitude south of the Hadley cell precluding it from facilitating dust lofting in the B storm. In fact, the zonal mean circulation indicates air is predominantly sinking over the south pole during the B storm. The thermally-direct polar cell (blue) in Figure 3 shows air is ascending over ∼75° S, traveling southward at ∼50 Pa, and descending over the south pole where the B storm is occurring. Thus, the mean overturning circulation provides little evidence for dust lofting during the B storm, which suggests the primary dust lofting mechanism is likely a process local to the south pole.

The MGCM shows the B storm is driven by repetitive dust plumes which inject dust above the boundary layer where dust radiative heating enhances convection and thereby maintains dust aloft in the middle atmosphere. One such dust plume is illustrated in Figure 4, which shows dust mixing ratio (shaded), shortwave (SW) heating rate (contoured), and net vertical velocities (combined vertical wind and sedimentation rate; arrows). Mixing ratios within the dust plumes are typically 6–8 ppm and can be as high as 14 ppm at the core of the most opaque plumes. Most of the plumes form in the eastern hemisphere, specifically around 100° E longitude, and travel westward for half a day before producing a detached dust layer. Detached layers have mixing ratios comparable to the dust plumes (6–8 ppm), although mixing ratios within the detached layers rarely exceed 10 ppm. Detached layers travel west for ∼12 hours before re-entering the eastern hemisphere where a new dust plume is typically developing.

The sizes of the dust plumes are largely consistent

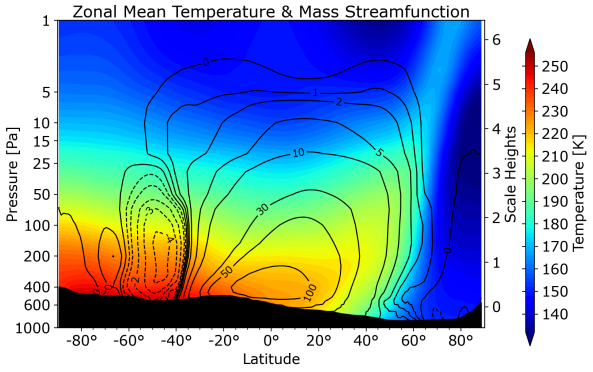

Figure 3: Zonal mean temperatures (color-filled) and mass streamfunction (MSF; contoured) during southern summer (L_s=255°–285°). From left to right, the MSF field shows a thermally-direct polar cell (blue) south of 75° S, a thermally-indirect midlatitude cell (orange) between 60°–75° S, a thermally-direct Hadley cell (blue) between 40°–60° S, the Hadley cell (orange), and a thermally-indirect polar cell (blue) poleward of 65° N.

throughout the duration of the B storm, with the exception that the plumes that form on the 2–3 days around solstice (L_s =270°) are the largest. The majority of B storm dust plumes are 3–4 scale heights tall, which places the uppermost part of the plume at around ∼10 Pa. However, the largest plumes can be up to 5 scale heights tall, around ∼3 Pa. The width of the dust plumes varies between ∼25°–100° in longitude, but most are ∼50° longitude wide. The detached dust layers produced by these plumes are located between 5–10 Pa and are no more than ∼25° of longitude wide. They tend to elongate over time as dust falls out of suspension.

The concentration of dust within a plume is highly correlated with the SW heating rate, especially above the boundary layer (∼1 scale height). SW heating rates are ∼30–45 K/day for mixing ratios between ∼6–8 ppm, and over ∼60 K/day for mixing ratios greater than ∼14 ppm. Positive (upward) net vertical velocities (with sedimentation rates subtracted) are ∼10–20 cm s^{-1} where SW heating rates >45 K/day (and, accordingly, mixing ratios >8 ppm), and can exceed ∼40 cm s^{-1} just above dust plumes and detached layers on the dayside of the planet.

The simulation suggests that the radiative-dynamic feedbacks caused by the presence of dust above the boundary layer are crucial to the B storm. In fact, in a simulation with radiatively inert transported dust the B storm does not occur. Figure 5 emphasises this point, showing the dust, vertical wind, and SW heating rate at L_s =270.19° as in Figure 4 but for the simulation in which transported dust is radiatively inert. There is no dust above the boundary layer in Figure 5, and in the absence of dust radiative heating, SW heating rates and positive net vertical velocities maximize around the longitude of local noon. However, even the strongest updrafts in this scenario are unable to loft dust above

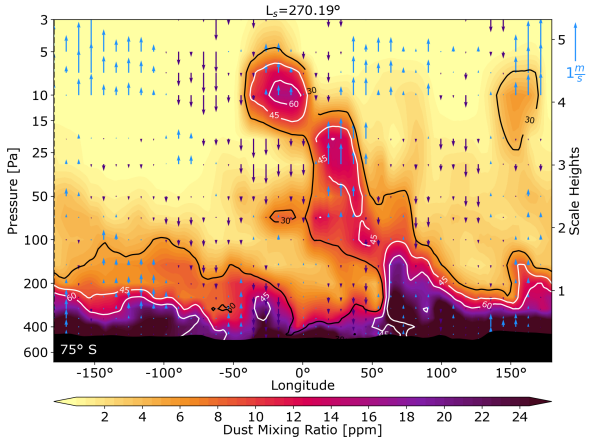

Figure 4: Simulated dust mixing ratio cross-section at 75 °S, L_s =270.19°. Dust mixing ratio is shaded, shortwave heating rate is contoured, vertical velocities (with dust sedimentation rates subtracted) are indicated by the arrows. Local noon is at ±180°.

the boundary layer, highlighting the importance of the dust radiative-dynamic feedback in producing the dust plumes.

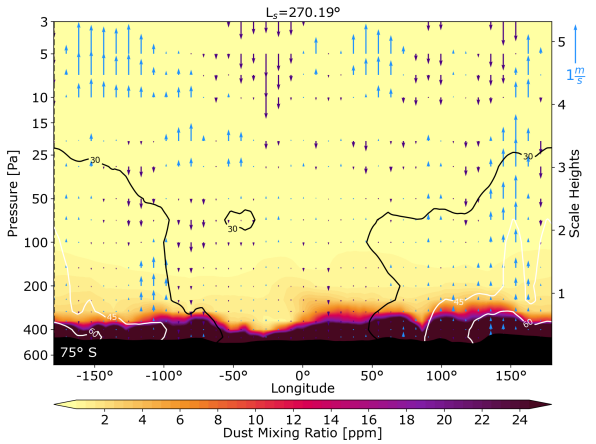

Figure 5: As in Figure 4 but for the radiatively inert dust case.

Conclusions and Future Work

The MGCM reproduces the B storm with middle-atmospheric temperatures and dust concentrations commensurate with observations. The simulated B storm is weaker than observed but has most of the characteristics of the observed B storms: zonal mean 50 Pa temperatures exceeding 200 K, zonal mean 50 Pa dust mixing ratios exceeding 4 ppm, peak intensity occurring at solstice (L_s =270°), and a short growth period followed by a long decay period.

The MGCM predicts that the B storm is comprised of westward-propagating dust plumes that form primarily in the eastern hemisphere and often produce detached dust layers. These dust plumes are self-sustaining: air-

borne dust absorbs and re-radiates heat, enhancing local convection and producing updrafts that maintain dust aloft. The pluming mechanism is responsible for lofting dust above the boundary layer thus creating the B storm. When the radiative effects of airborne dust are excluded from the simulation, dust does not plume up above the boundary layer and the B storm never develops. Now that we have identified the pluming mechanism in the simulation, we intend to revisit the MCS data to look for evidence of dust pluming in the observations.

The hours-long lifespan of a dust layer lofted in a plume and later advected around the planet as a detached dust layer, coupled with the dependency of the lofting mechanism on the radiative heating of suspended dust particles, suggests that the "solar escalator" as described in [2] may be occurring. The solar escalator is so named for the step-like trajectory of a dust layer ascending over a period of several days, which is caused by the differential heating of the dust layer throughout a diurnal cycle [2]. We are in the process of performing a trajectory analysis on the dust plumes in our simulation and we will assess the importance of this mechanism for the evolution of the B storm.

References

[1] Bertrand, T. et al., 2020. Simulation of the 2018 global dust storm on Mars using the NASA Ames Mars GCM: A multi-tracer approach. *J. Geophys. Res.*, 125(7)

[2] Daerden, F. et al., 2015. A solar escalator on Mars: Self-lifting of dust layers by radiative heating. *Geophys. Res. Lett.*, 42:7319–7326

[3] Haberle, R. et al., 2019. Documentation of the NASA/Ames Legacy Mars Global Climate Model: Simulations of the present seasonal water cycle. *Icarus*, 333:130–164

[4] Haberle, R. M., 1986. Interannual variability of global dust storms on Mars. *Science*, 234(4775):459–461

[5] Kass, D. et al., 2016. Interannual similarity in the Martian atmosphere during the dust storm season. *Geophys. Res. Lett.*, 43:6111–6118

[6] Montabone, L. et al., 2015. Eight-year climatology of dust optical depth on Mars. *Icarus*, 251:65–95

[7] Smith, D. et al., 1999. the global topography of Mars and implications for surface evolution. *Science*, 284(5419):1495–1503

[8] Smith, M. et al., 2017. Thermal structure and composition. In R. Haberle, R. Clancy, F. Forget, M. Smith, & R. Zurek, eds., *The Atmosphere and Climate of Mars*, chap. 4, 42–75, Cambridge University Press, New York, NY2017

[9] Toon, O. et al., 1989. Rapid calculation of radiative heating rates and photodissociation rates in inhomogenous multiple scattering atmospheres. *J. Geophys. Res.*, 94(D13):16287–16301

[10] Wilson, R. et al., 2007. Diurnal variation and radiative influence of Martian water ice clouds. *Geophys. Res. Lett.*, 34(2)

[11] Wolff, M. et al., 2017. Radiative processes: Techniques and applications. In R. Haberle, R. Clancy, F. Forget, M. Smith, & R. Zurek, eds., *The Atmosphere and Climate of Mars*, chap. 6, 106–171, Cambridge University Press, New York, NY2017